Supporting Information

On-chip clonal analysis of glioma stem cell motility and therapy resistance

Daniel Gallego-Perez,[1, 2, 3, 4†] Lingqian Chang,[2, 3†] Junfeng Shi,[3, 5] Junyu Ma,[3] Sung-Hak Kim,[6] Xi Zhao,[3, 7] Veysi Malkoc,[3, 7] Xinmei Wang,[3, 7] Mutsuko Minata,[6] Kwang J. Kwak,[3, 7] Yun Wu,[3] Gregory P. Lafyatis,[8] Wu Lu,[9] Derek J. Hansford,[2, 3] Ichiro Nakano,[6] and L. James Lee[3, 4, 7]*

[1] The Ohio State University, Department of Surgery, Columbus, OH 43210

[2] The Ohio State University, Department of Biomedical Engineering, Columbus, OH 43210

[3] The Ohio State University, Center for Affordable Nanoengineering of Polymeric Biomedical Devices, Columbus, OH 43210

[4] The Ohio State University, Center for Regenerative Medicine and Cell-Based Therapies, Columbus, OH 43210

[5] The Ohio State University, Department of Mechanical Engineering, Columbus, OH 43210

[6] University of Alabama at Birmingham, Department of Neurosurgery, Birmingham, AL 35294

[7] The Ohio State University, Department of Chemical and Biomolecular, Columbus, OH 43210

[8] The Ohio State University, Department of Physics, Columbus, OH 43210

[9] The Ohio State University, Department of Electrical and Computer Engineering, Columbus, OH 43210

[†] Equal contribution

*To whom correspondence should be addressed: lee.31@osu.edu

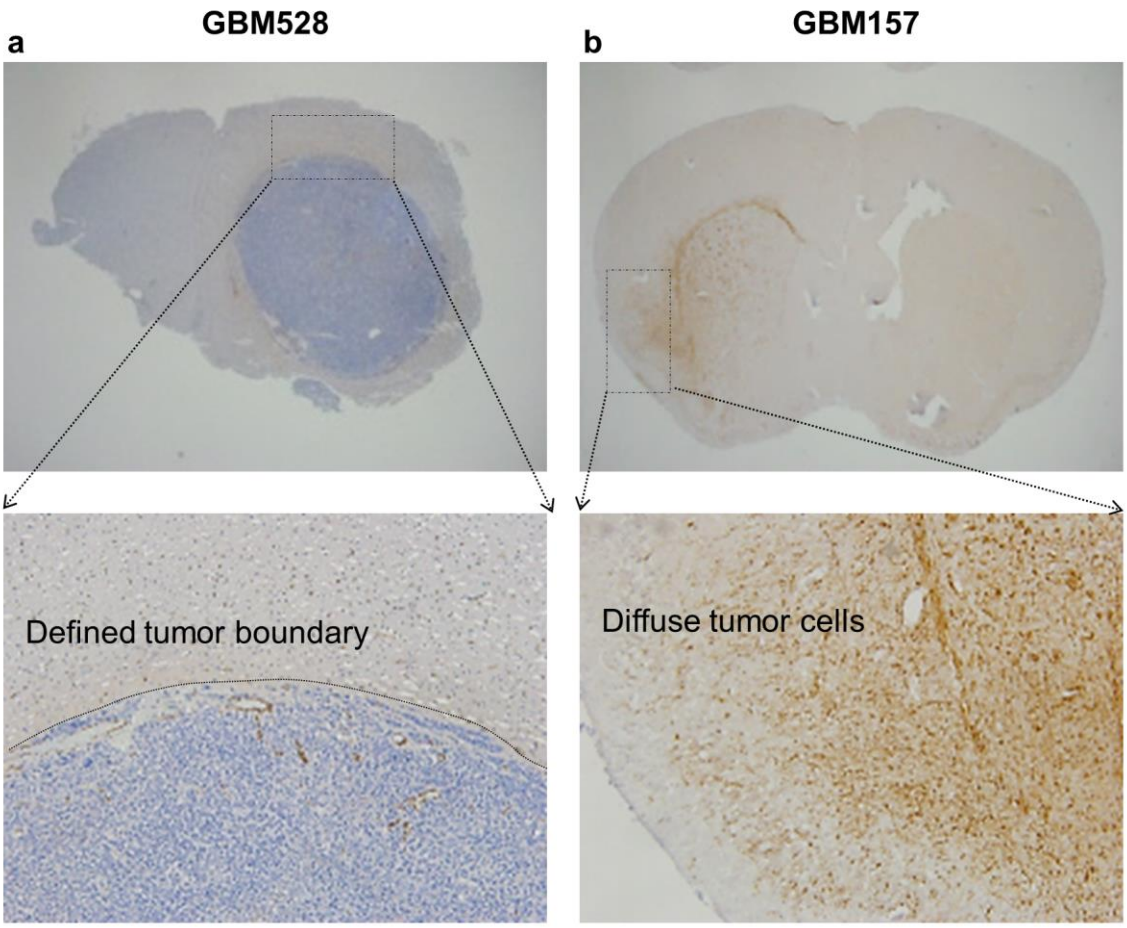

Figure S1. Patient-derived GSCs exhibit different dissemination capabilities in a xenograft mouse model. (a) GBM528 form a tumor with defined boundaries with little to no signs of active cell infiltration. **(b)** GBM157 form tumors with diffuse boundaries, indicative of active cell migration/dissemination.

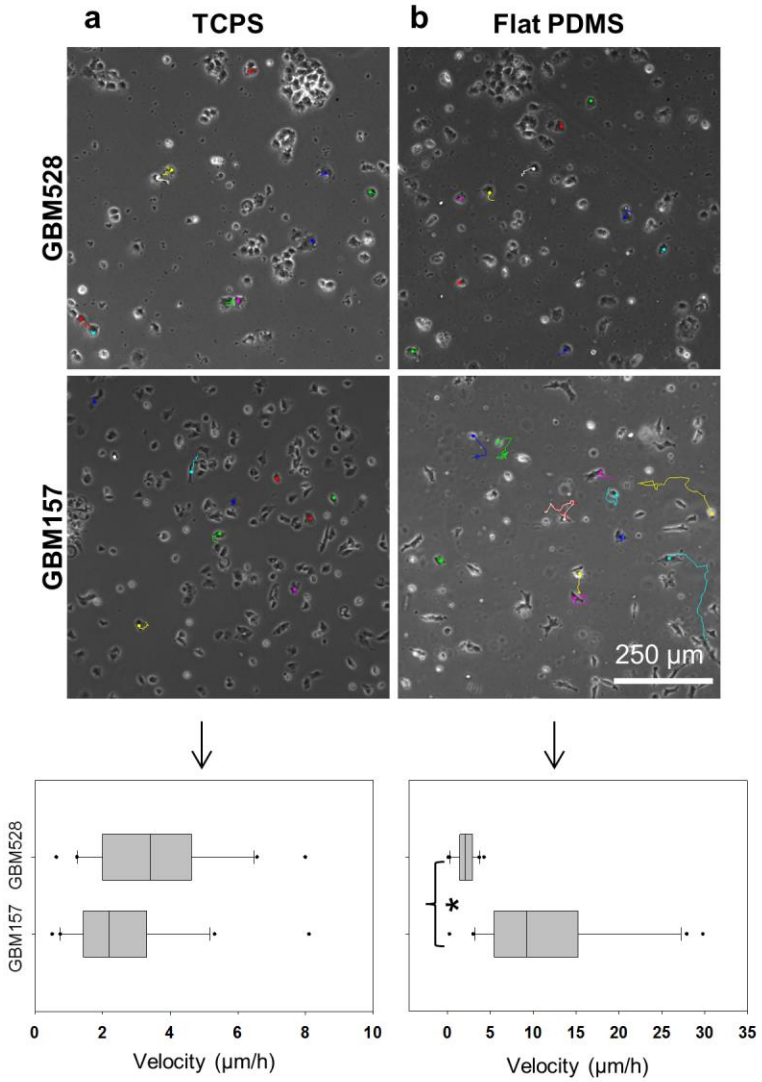

Figure S2. Single cell motility of GSCs on flat surfaces. (a) Both GBM157 and GBM528 populations show significantly reduced motility when assayed on a flat tissue culture polystyrene (TCPS) surface. **(b)** Single-clone motility increases for GBM157 when assayed on a softer PDMS surface, thus correlating better with their observed behavior *in vivo*. GBM528, on the other hand, did not show an increase in motility. * $p<0.05$ (Dunn's Method).

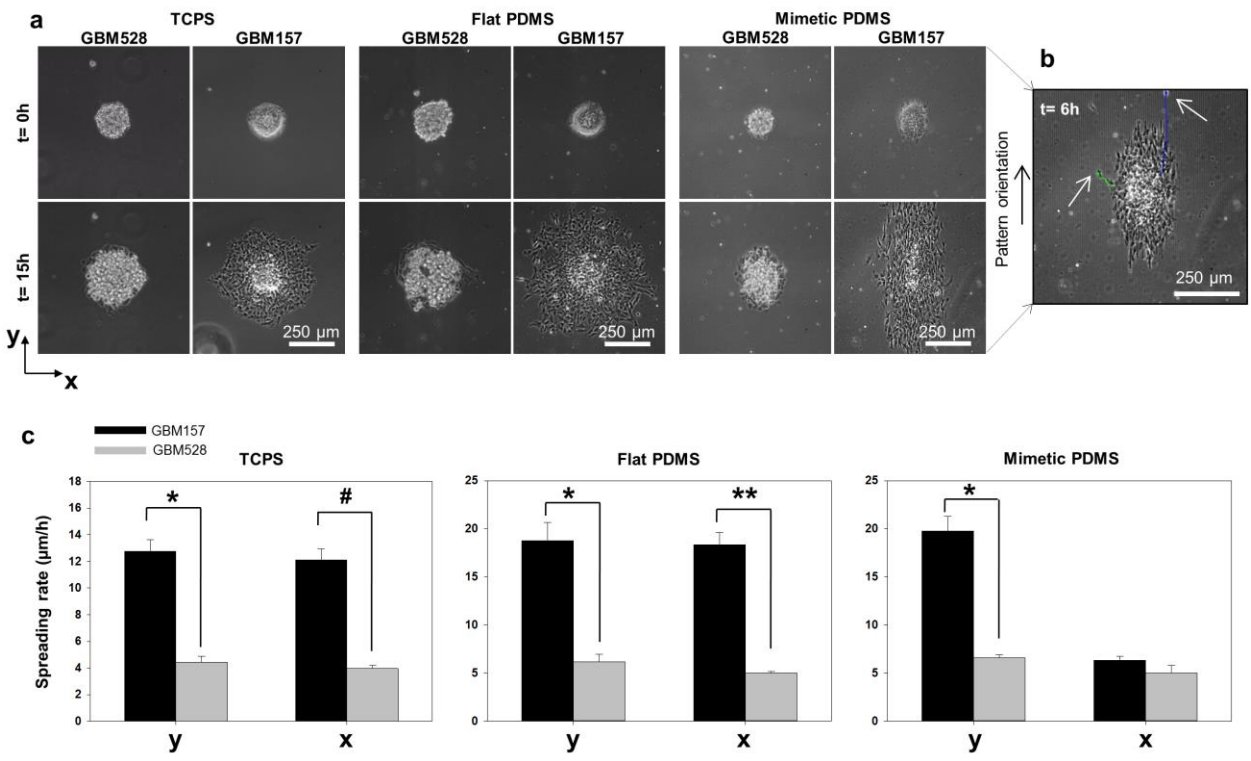

Figure S3. GSC motility analysis at the spheroid level. (a) Spheres derived from GBM157 GSCs exhibit enhanced spreading capabilities compared to spheres derived from GBM528 GSCs. GBM157 spheres showed asymmetric spreading along the "y" axis on patterned/mimetic surfaces, as determined by the orientation of the topography on the surface. GBM528 spheres on the other hand still showed a relatively symmetric spreading pattern, thus indicating that they are less responsive to topographical/structural cues compared to GBM157 GSCs. **(b)** Single GBM157 GSCs are seen migrating out of the sphere at a much faster rate compared to the bulk of the population. **(c)** Quantification of the spreading rate on different surfaces. GBM157 spheres show a slight increase in dissemination capabilities when cultured on softer PDMS surfaces compared to TCPS. GBM528 spheres showed similar spreading capabilities on both surfaces. GBM157 spheres show enhanced spreading capabilities along the "y" axis. * $p<0.05$ (Holm-Sidak method), # $p<0.05$ (Tukey Test), ** $p<0.05$ (Dunn's Method).

We compared the migratory/spreading behavior of GBM157 and GBM528 GSC spheres on three different test surfaces: conventional tissue culture polystyrene (TCPS), flat polydimethylsiloxane (PDMS), and micropatterned/biomimetic PDMS. Our findings on TCPS and flat PDMS (**Figure S3**, left and middle, respectively) show that GBM157 and GBM528 spheres spread symmetrically on these surfaces. Both cell populations exhibited some degree of bulk motility, with GBM157 spheres being able to spread at a faster rate ($p<0.05$) compared to GBM528 spheres (**Figure S3e**). Interestingly, spheres derived from GBM157 were also able to spread more rapidly ($p<0.05$) on the softer PDMS surface compared to TCPS. Spheres derived from GBM528, on the other hand, showed similar spreading capabilities on both TCPS and flat PDMS.

The behavioral differences between GBM157 and GBM528 spheres became more pronounced when plated on patterned/biomimetic PDMS surfaces (**Figure S3c**, right). The behavior of GBM157 spheres was clearly influenced by the underlying topography, as evidenced by asymmetric spreading along the pattern direction, clearly establishing a preferential 'y' *vs*. 'x' axis of dissemination. Spheres from GBM528 still spread symmetrically regardless of pattern orientation. Similarly, GBM157 spheres showed a tendency to disseminate throughout the surface at a faster rate ($p<0.05$) compared to GBM528 spheres (**Figure S3e**). Altogether, these observations suggest GBM528 spheres seemed to have an intrinsic predisposition to spread at a relatively constant and slow rate on all surfaces independent of chemistry, mechanical properties, and topography. On the other hand, GBM157 spheres clearly altered their spreading pattern in response to changes in these variables, which is indicative of their ability to potentially sense and

respond to cues in their *in vivo* microenvironment, and further highlights heterogeneities across patient-derived GSC populations.

Although for the most part sphere spreading on the biomimetic PDMS surfaces was also due to motility of the bulk population, subsets of single GBM157 clones could be seen migrating out of the spheres at a much faster rate compared to the bulk of the population (**Figure S3d**, arrows). Such behavior presumably resembles more closely the *in vivo* dissemination patterns exhibited by invasive GSCs. In contrast, no single-clone motility was detected in GBM528 spheres, thus suggesting that these cells show limited dissemination potential *in vivo*.

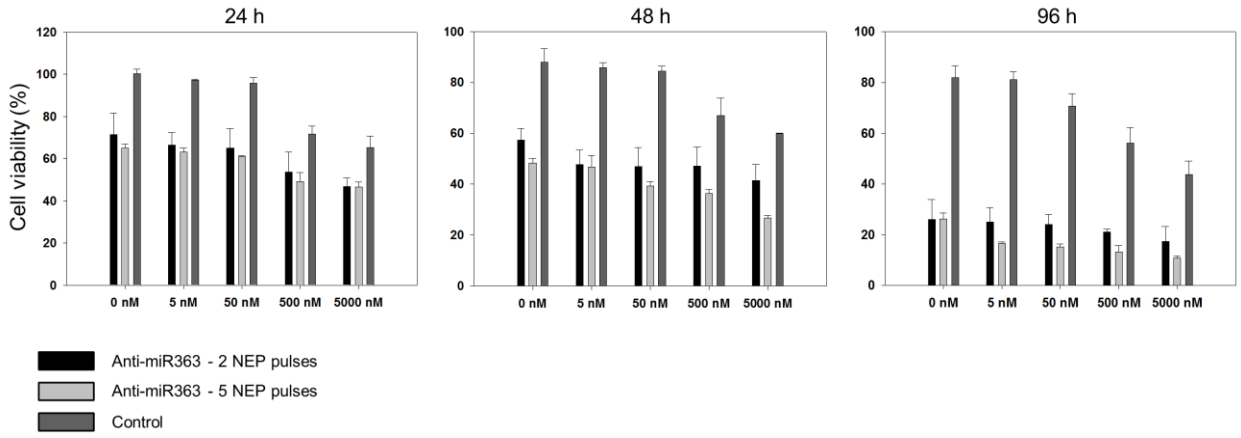

Figure S4. Expanded data on therapy efficacy studies at different timepoints. Cell death increases in proportion to the concentration of Temozolomide and/or the dose of anti-miR363 delivered by 3D NEP.

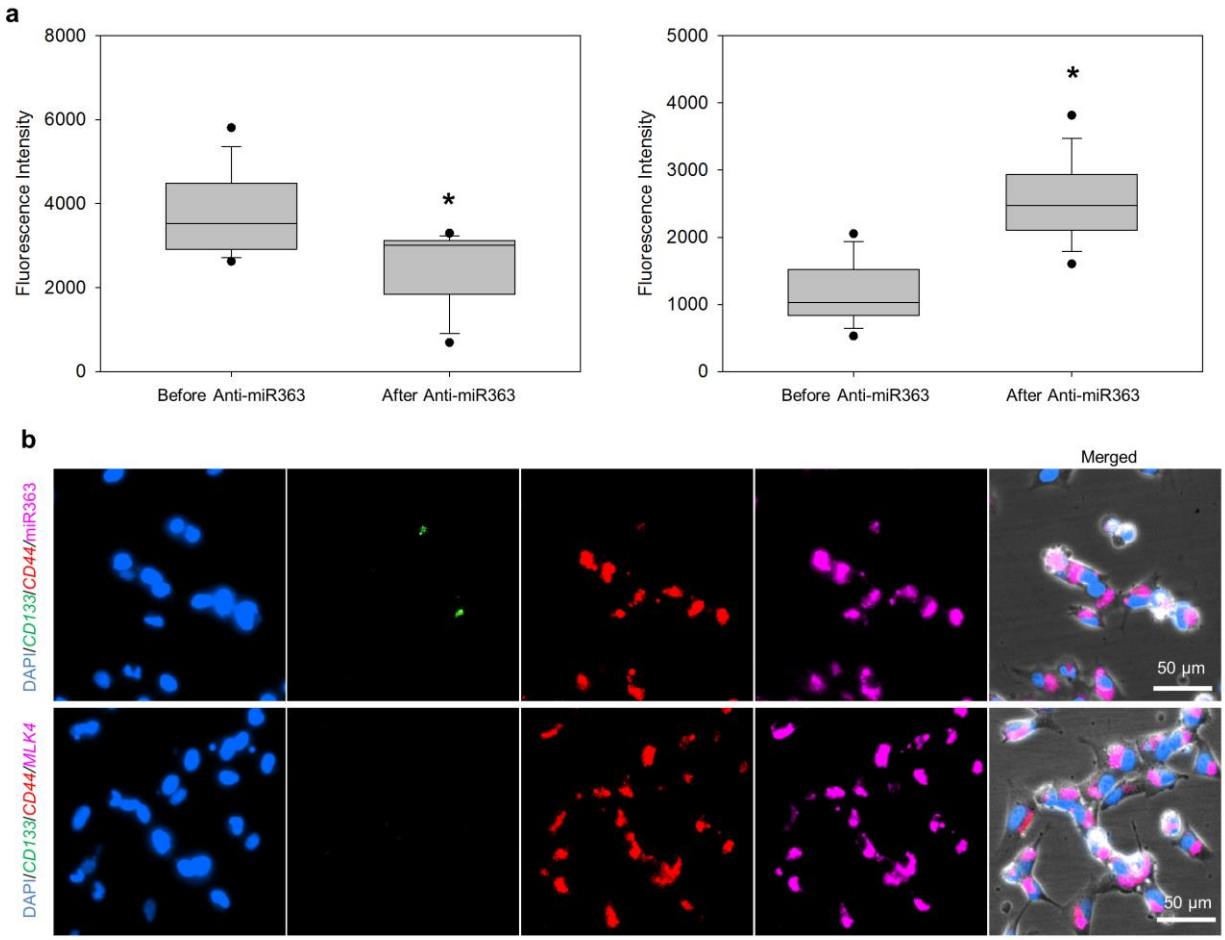

Figure S5. NEP/MB-based detection of multi-gene-expression and oligo RNA. (a) Quantification of miR363 and *MLK4* expression before and after anti-miR363 delivery. The levels of miR363 in the surviving cell population decreased as expected. The Levels of *MLK4*, on the other hand, increased, which further suggests that the surviving cell population has a more mesenchymal-like phenotype. **(b)** Fluorescence micrographs showing multi-gene and oligo RNA detection capabilities in the surviving cell population, which has low/negligible expression of proneural marker *CD133*, and high expression of mesenchymal markers *CD44* and *MLK4*. * $p<0.05$ (Mann–Whitney rank sum test).

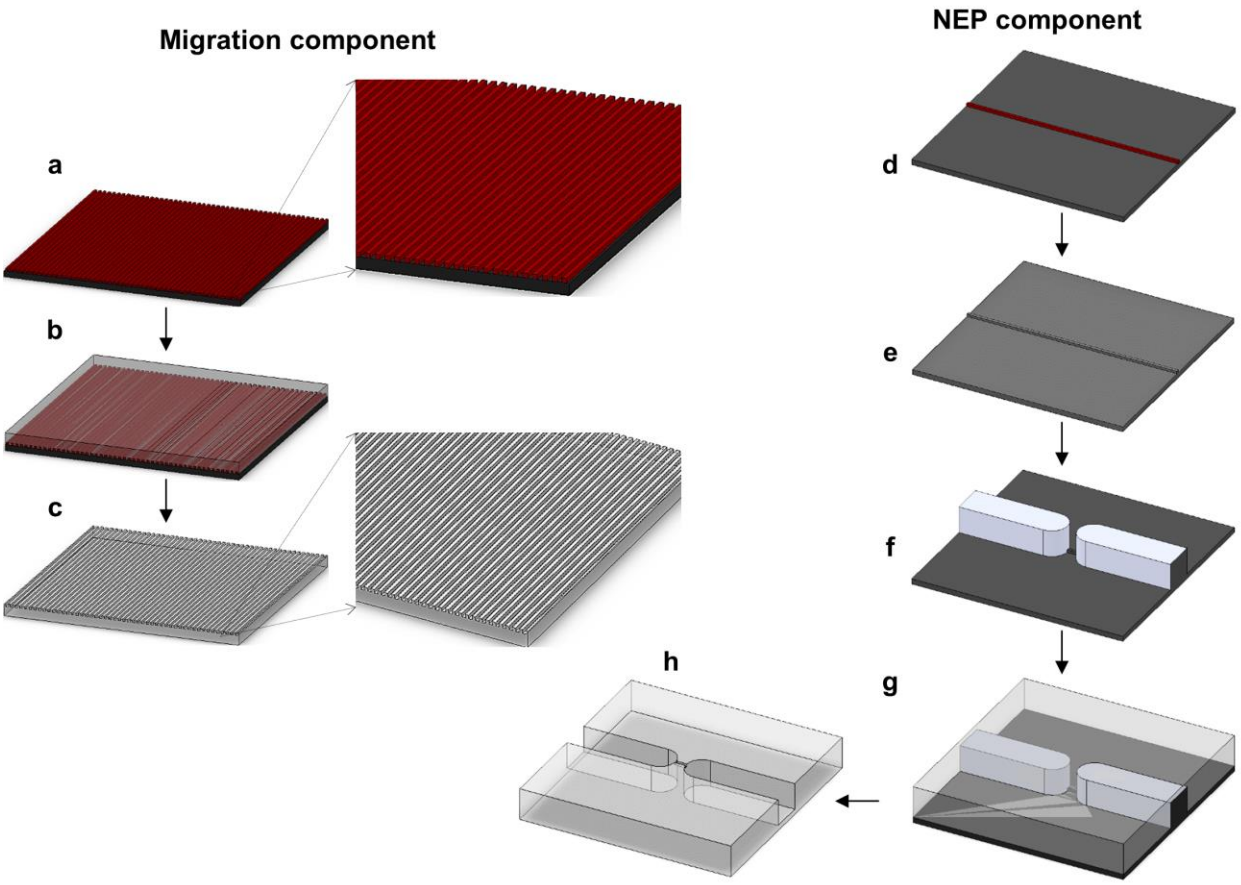

Figure S6. Fabrication schematics. (a-c) Migration component: **(a)** Photolithographically-patterned Si wafer, **(b)** PDMS casting, **(c)** PDMS demolding. **(d-h)** NEP component: **(d)** SPR950 nanowire on Si, **(e)** Si etching, **(f)** Aligned SU-8 patterning, **(g)** PDMS casting, **(h)** PDMS demolding.